Investigation of the paramagnetic rare-earth oxide Nd_2O_3 by muon spin spectroscopy

R C Vilão,[1, *] M A Curado,[1, 2] H V Alberto,[1] J M Gil,[1] J A Paixão,[1] J S Lord,[3] and A Weidinger[4]

[1]CFisUC, Department of Physics, University of Coimbra, P-3004-516 Coimbra, Portugal
[2]International Iberian Nanotechnology Laboratory, P-4715-330 Braga, Portugal
[3]ISIS Facility, Rutherford Appleton Laboratory, Chilton, Didcot, Oxon OX11 0QX, United Kingdom
[4]Helmholtz-Zentrum Berlin für Materialien und Energie,
Institute for Nanospectroscopy, D-12489 Berlin, Germany
(Dated: August 26, 2019)

In the context of a systematic study of oxide materials with the muon spin spectroscopy (μSR) technique, we report here on an investigation of paramagnetic Nd_2O_3. The question was whether the magnetism of Nd^{3+} has an influence on the observed signals. In Nd_2O_3, as in the other oxides, a weakly paramagnetic component is observed besides the pure diamagnetic fraction. The paramagnetic part is assigned to a transient state formed between the initial atomic and the final bound muonium configuration. In addition, a fast relaxing signal ($\lambda \sim 7~\mu s^{-1}$) with 10 to 20% fraction is seen in longitudinal field. Contrary to this general behavior of the oxide materials, in the present magnetic compound, a resonance-like structure is seen in the temperature range around 40 K. We assign it tentatively to a dynamical process related to the population of the first excited Kramers doublet of the Nd^{3+} ion at 2.6 meV.

I. INTRODUCTION

Oxides with trivalent rare-earth cations, of the general sesquioxide form R_2O_3, play an important role in solid state physics and materials science. Due to the incomplete filling of the metal atom shells, sesquioxides present a rich field for technological research and applications.[1–6] In fact, as rare-earth-sesquioxides can present more than one crystal structure, for particular temperature and pressure conditions, they may exhibit several phases (spin, charge, orbital states), which can enhance the diversity in potential applications. Among rare earth-sesquioxides, Nd_2O_3 assumes a prominent role in photonic applications, as a candidate high$-\kappa$ dielectric, in sensor or catalyst applications.[7–13]

The hydrogen impurity is mostly unavoidable within materials and can have a deep impact in the properties of semiconductors and insulators , particulary in the electrical properties. Hydrogen is known to passivate impurities or defects in semiconductors, but isolated hydrogen can also act as a dopant or as compensating amphoteric impurity.[14–16] The knowledge of the isolated hydrogen configurations inside the material is of fundamental importance in order to understand the electrical properties.[17,18]

Nd_2O_3 is no exception and the growth methods for this rare-earth sesquioxide imply the possibility of introduction of the hydrogen impurity in high concentrations.[11,19,20] Thin-films of Nd_2O_3 grown by atomic layer deposition present hydrogen concentration as high as 1.2%.[20] However, little is known about the effect of hydrogen in Nd_2O_3.

The investigation of the configurations of isolated hydrogen in semiconductors and oxides has known an intensive contribution from the experimental results obtained by muon spin spectroscopy (μSR) on muonium.[15,16,21] This atom formed by an electron bound to a positive muon can be thought in condensed matter physics and chemistry as a light pseudo isotope of hydrogen, due to the near coincidence of its electronic properties.[22] The implantation of positive muons allows to probe the ground state as well as transient metastable configurations of muonium, which allows to clarify many microscopic aspects of the hydrogen dynamics inside the material.[23–26]

Muon spectroscopy studies of muonium as a pseudo isotope of hydrogen are however generally undertaken in diamagnetic materials. The muon being a very sensitive magnetic probe, the existence of paramagnetism may impact on the μSR signal. The presence of the paramagnetic Nd^{3+} ions in Nd_2O_3 therefore brings the additional challenge of separating the effect of the paramagnetic ions on the usual signals of the different muonium configurations in this paramagnetic oxide.

In insulating and semiconducting oxides, two main signals are usually observed in μSR studies: precession of the muon spin at the characteristic Larmor frequency of the bare muon are typically assigned to positively charged muonium Mu^+ bound to oxygen, corresponding to the hydrogen donor configuration.[27,28] Precession of the muon spin with the characteristic frequencies of neutral muonium are assigned to neutral muonium Mu^0, typically in interstitial locations corresponding to the hydrogen acceptor configuration(s),[25,29] seldom observed in its negatively charged state Mu^-.[30] The muon being an implanted probe, the characteristic signals may be either washed-out in the thermalization process (missing fraction) or transient signals may be visible.[30–32]

The present work represents the first successful attempt to characterise the characteristic muonium configurations in a strongly paramagnetic oxide.
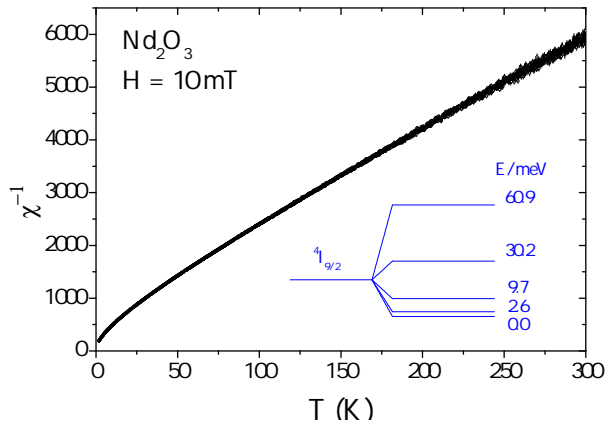
FIG. 1: Temperature dependence of the inverse magnetic susceptibility of Nd_2O_3, for an external applied magnetic field H= 10 mT. The inset shows the well-known lift-up of the degeneracy of the 10-fold $^4I_{9/2}$ ground state of the Nd^{3+} paramagnetic ion due to the effect of the crystal field.

II. EXPERIMENTAL DETAILS AND RESULTS

A high-purity polycristalline sample of Nd_2O_3 was used (obtained commercially from Alfa Aesar, REacton, 99.999%) in this work. Nd_2O_3 crystallizes in the hexagonal La_2O_3 structure (A-type, space-group P3m1, no.164).[33]

Conventional magnetometry measurements were undertaken at the TAIL Facility of the University of Coimbra: the temperature dependent inverse magnetic susceptibility of our sample (subject to an external magnetic field B = 0.01 T) is shown in Fig. 1. The temperature dependence of the susceptibility at high-temperatures is well described by a Curie-Weiss model with the expected magnetic moment for the Nd^{3+} ion. The deviation at low-temperatures is a well-known crystal field effect associated to the lift up of the degeneracy of the $J = 9/2$ ground state multiplet.[34] The corresponding energy levels are shown as an inset in Fig. 1.[35]

Muon spin spectroscopy experiments were performed at the EMU instrument of the ISIS Facility at the Rutherford-Appleton Laboratory (United Kingdom). Conventional muon spin rotation measurements were undertaken from T = 8 K up to T = 640 K with an applied transverse magnetic field B = 0.01 T. Longitudinal field measurements were also performed at room temperature. Calibration of the maximum asymmetry of the instrument was obtained using a silver sample.

A. μSR time spectra

Figure 2 shows the experimental μSR time spectrum at low transverse field (0.01 T) at the temperature of 100 K. The oscillation frequency corresponds to the Lar-
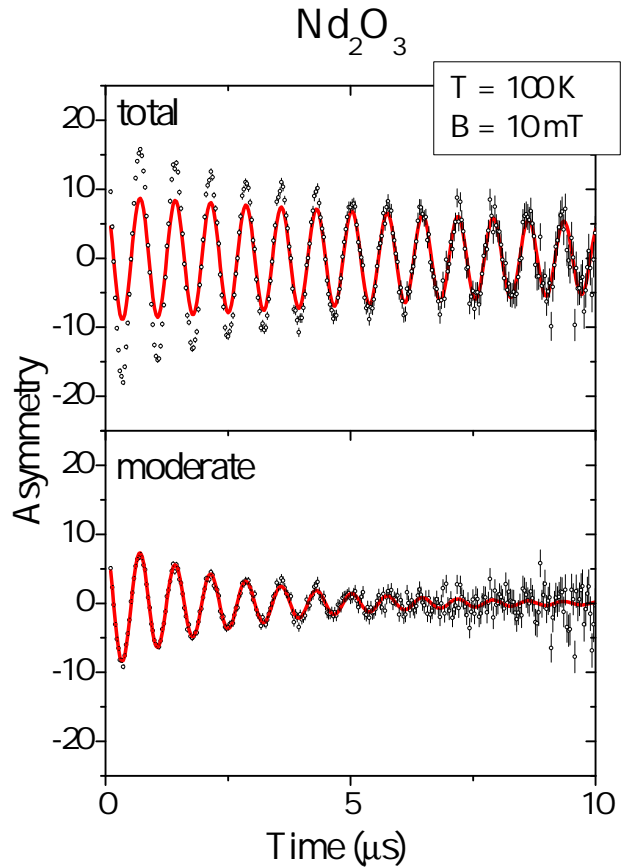

FIG. 2: Transverse field time spectrum at T = 100 K and B = 10 mT. Two relaxations can be distinguished: Slow $(0.05(1)\ \mu s^{-1})$ and moderate $(0.38(3)\ \mu s^{-1})$. The total asymmetry is shown in the upper pannel, together with the fitted slow relaxing component (red line). The moderately relaxing component is shown in the lower pannel.

mor precession frequency expected for the diamagnetic (bare) muon. However, the spectrum shows clearly two components, distinguished by the relaxation rate. The slow component (red line in the upper frame of Fig. 2) relaxes with a rate of $\lambda = 0.05(1)\ \mu s^{-1}$ (due to nuclear moments) and is assigned to muons in a diamagnetic environment.

The difference between the total spectrum and the diamagnetic component is displayed in the lower frame of Fig. 2. The relaxation rate of this curve ($\lambda = 0.38(3)\ \mu s^{-1}$) indicatives that a paramagnetic interaction with an unpaired electron is involved. Similar signals were observed in many other systems.[36–38] We assign this moderately relaxing signal (moderate to distinguish it from fast, see below) to a transition state which is formed as an intermediate configuration between incoming atomic muonium and the final bound configuration (for details see Ref. 30).

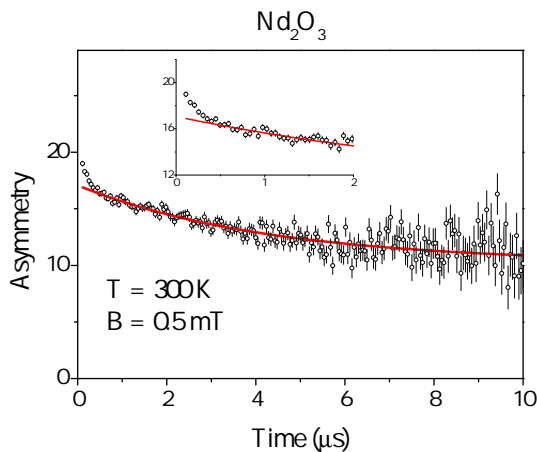We have also measured a longitudinal field decoupling

FIG. 3: Longitudinal field time spectrum at T = 300 K and B = 0.5 mT. The sum of the constant and moderately relaxing (λ = 0.38(3) μs^{-1}). components is showed as a red line. The insert shows the first two microseconds of the spectrum, together with a fit including the fast component as well (blue line, λ = 7(1) μs^{-1}).

curve at 300 K. A low-field time spectrum is shown in Fig. 3. The weakly relaxing main component (red solid line) is decomposed in a constant (decoupled) fraction and a slowly relaxing component. The origin of the later is not clear. It may contain some contribution from the moderately relaxing signal discussed in connection with Fig. 2, but this signal is very weak at 300 K. The main part of the slowly relaxing component is thus attributed to background or an instrumental effect. We do not discuss the weakly relaxing signal (solid line in Fig. 3) any further.

The main emphasis in connection with Fig. 3 lies on the fast signal ($\lambda \sim 7$ μs^{-1}) which is displayed separately in the insert of the figure. The amplitude (ca. 20% fraction) and the relaxation are fairly constant up to longitudinal fields well above 0.1 T. This indicates that a fairly large hyperfine interaction in the order of atomic muonium is involved. We assign the fast signal to delayed conversion of the incoming (excited) muonium to ground state muonium, possibly via a diamagnetic-like transition state.[30] The fast signal is, due to dephasing, not seen in the transverse field experiment and constitutes the major part of the missing fraction in Fig. 2 and Fig. 4.

B. Temperature dependence

In order to obtain an overview of the data we analyzed the transverse field measurement with a single frequency without distinguishing between the moderately and slowly relaxing signal. The fit parameters (fraction, relaxation rate, frequency and phase) are displayed in Fig. 4.

A remarkable feature of data is the resonance-like behavior at about 40 K. We discuss this part separately
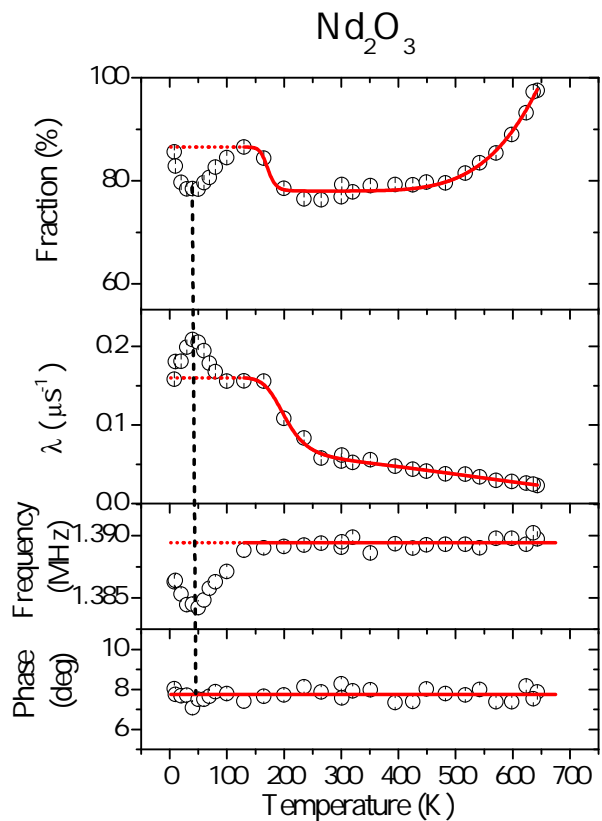

FIG. 4: Diamagnetic-like component at a transverse magnetic field of B = 10 mT: Fraction, relaxation (λ), frequency, and phase from one-component analysis. The red lines mark the overall behavior of the parameters without the resonance-like feature at about 40 K.

below. The rest of the data, indicated by the red lines, shows a behavior similar to other oxides.[31,36,37,39] The fraction amounts to about 80% of all muons for the major part of the temperature range. At the highest temperatures above 500 K full recovery sets in. Below 200 K, the fraction increases by about 10%. The slightly higher fraction at low temperatures is attributed to a thermal spike effect described in a recent paper.[32] We suggest that muonium in the unrelaxed lattice is very reactive and can overcome the reaction barrier in a similar way as thermal excitation induces the reaction at higher temperature. This extra excitation energy disappears with increasing temperature due to thermal conduction, leading to a drop in the fraction.

The relaxation rate shows a strong decrease in the temperature range between 150 and 250 K. This decrease is attributed to the delayed conversion of the paramagnetic to the diamagnetic configuration. The frequency and phase are fairly constant outside the resonance region and correspond to the values of the calibration mea-

surement.

Thus, three special phenomena are observed and will be discussed below. These are:

1. Recovery of the diamagnetic fraction above 500 K.

2. Conversion from paramagnetic to diamagnetic configuration around 200 K.

3. Resonance-like behavior at 40 K.

III. DISCUSSION

The μSR signal of this experiment is basically diamagnetic, i.e. the precession frequency corresponds approximately to the Larmor frequency of the muon spin. However, the relaxation at low temperatures (ca. $0.38~\mu s^{-1}$) is larger than expected for the bare muon (ca. $0.05~\mu s^{-1}$), indicating an interaction with an unpaired electron. The larger relaxation disappears around 200 K due to the loss of the paramagnetic electron (ionization).

A. Full recovery of the diamagnetic fraction above 500 K

The increase of the fraction above 500 K is attributed to ionization of the missing fraction part. The activation energy amounts to 0.4(1) eV. This recovery is usually assigned to the thermal ionization of ground state muonium. However, this is not completely unambiguous. It is also possible that ionization takes place from some excited configuration before the ground state is formed. Then the 0.4 eV represent only a lower limit of the ionization energy of ground state muonium.

B. Conversion from paramagnetic to diamagnetic around 200 K

We assume that the strong change of the relaxation in Fig. 4 between 150 and 250 K is due to the delayed conversation of the weakly-paramagnetic to the diamagnetic configuration. Thus, for an individual muon the spin precession relaxes first with the rate $\lambda_e + \lambda_n$ and after some time with the rate λ_n. The rate λ_e is due to the interaction of the muon spin with the paramagnetic electron and λ_n to the interaction with nuclear spins. In the paramagnetic configuration both interactions are present, thus the sum of the two relaxation rates has to be taken.

The ensemble averaging over all conversions with a mean conversion time τ yields for the polarization function:

$$
\begin{aligned}
P(t) =& a_1 \left(1 - \frac{1}{\lambda_e \tau + 1} \right) \times \\
& \exp \left[-\left(\lambda_e + \lambda_n + \frac{1}{\tau} \right) t \right] \cos(\omega t) \\
&+ a_1 \frac{1}{\lambda_e \tau + 1} \exp(-\lambda_n t) \cos(\omega t)
\end{aligned} \tag{1}
$$

a_1 is the fraction taking part in the conversion. $P(t)$ has the form (without the cos-term):

$$
\begin{aligned}
P(t) =& f_{\text{para}} \exp \left[-\left(\lambda_e + \lambda_n + \frac{1}{\tau} \right) t \right] \\
&+ f_{\text{dia}} \exp(-\lambda_n t)
\end{aligned} \tag{2}
$$

The relaxation of the paramagnetic fraction contains the contribution $1/\tau$ from lifetime broadening.

The μSR time spectra were fitted with Eq. 1, assuming $\lambda_n = 0.05(1)~\mu s^{-1}$, the value obtained by the fit of the spectrum in Fig. 2, and treating a_1, λ_e and τ as free parameters. In the transition region around 200 K, λ_e was fixed to the value obtained at lower temperatures to avoid ambiguities. Figure 5 shows in the upper frame the fractions f_{para}, f_{dia} and $f_{\text{tot}} = f_{\text{para}} + f_{\text{dia}}$ as function of temperature. In the lower frame the relaxation rate of the moderately relaxing paramagnetic signal is displayed. This relaxation has two contributions, one ($\lambda_0 = \lambda_e + \lambda_n$) caused by the distribution of internal fields and the other ($1/\tau$) caused by lifetime broadening.

In this analysis the decrease of the paramagnetic fraction equals the increase of the diamagnetic fraction. In the conversion region, the relaxation rate of the paramagnetic signal increases due to lifetime broadening. Thus the disappearance of the paramagnetic signal has two reasons, the decrease of the fraction and the increase of the relaxation rate. The two phenomena are correlated via the mean conversion time τ. In the past, the separation of these phenomena posed problems and often either the fraction ((Ref. 40)) or the relaxation (Ref. 37) was kept constant and only the other parameter was varied. The correlated approach used here gives a more adequate description of the conversion process.

We assumed in the above analysis that the diamagnetic fraction is completely due to the delayed conversion (ionization) of the paramagnetic configuration. However, part of the diamagnetic fraction may be formed promptly or at least on a different time scale than the diamagnetic fraction resulting from conversion. In the above analysis we did not distinguish between these two contributions.

C. Resonance at 40 K

As seen in Fig. 4, a resonance-like structure shows up at around 40 K: The relaxation rate is increased and the fraction and frequency are decreased, the phase is little
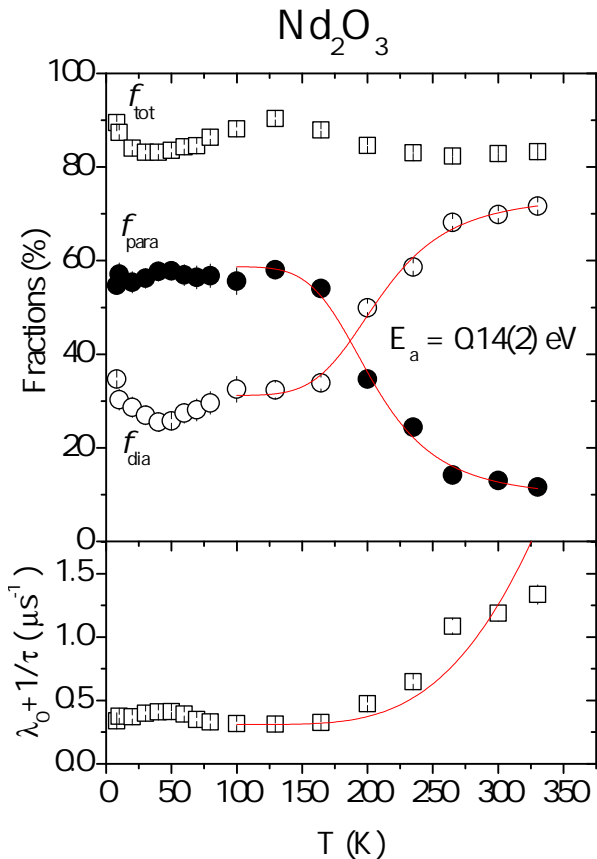
FIG. 5: Temperature dependence of the fractions f_{dia}, f_{para} and $f_{tot} = f_{dia} + f_{para}$, highlighting the conversion of the paramagnetic to diamagnetic fraction in the temperature region around 150 to 250 K. The fractions are shown in the upper frame and the relaxation rate of the moderately relaxing signal is shown in the lower frame. The relaxation of this component is caused by a distribution of internal fields ($\lambda_0 = \lambda_e + \lambda_n$) and the contribution $1/\tau$ from lifetime broadening. The fit curves correspond to an activation energy of 0.14(2) eV.

effected. This experimental feature (peak- and dip-like behavior) is indicative of a spin-lattice (T_1) resonance effect. The present transverse field geometry is not well suited to measures T_1 processes. However, in case of strong coupling of the muon spin with the surrounding electronic system, T_1 relaxation may give rise to the observed effects. We assume for the analysis that a fluctuating spin-lattice interaction comes into resonance with the Larmor precession of the muon spin. Then the $1/T_1$ relaxation rate has the following dependence:

$$\frac{1}{T_1(\mu)} \propto \frac{\tau_c}{1 + (\omega_L \tau_c)^2} \tag{3}$$

with $\omega_L = \gamma_\mu B_{ext}$ and τ_c the correlation time. This yields at the peak position:

$$\omega_L \tau_c \, (T = 40\,\text{K}) = 1$$
$$\Rightarrow \tau_c \, (T = 40\,\text{K}) = \frac{1}{\gamma_\mu B_{ext}} = 0.74\,\mu s \tag{4}$$

Thus, a fairly slow dynamical process is involved which certainly does not correspond to the thermal fluctuation of the Nd moments. However, the low-lying Nd^{3+} spin states are grouped in Kramers doublets and the first excited doublet lies only 2.6 meV above the ground state[35] and thus becomes appreciably populated at 40 K. Since the effective magnetic moments of the ground and excited state are different one obtains a fluctuating hyperfine interaction which may cause the T1 relaxation of the muon spin. In this interpretation, the resonance at 40 K in the present experiment is attributed to the excitation and de-excitation of the Nd^{3+} first excited Kramers doublet with a rate in the order of $1/(0.74\,\mu s)$ at 40 K.

Another dynamical process is the site change of the weakly bound electron with respect to the muon position. This will lead to a fluctuating hyperfine interaction with different values and orientations and could give rise to a T_1 resonance in both magnetic and non-magnetic materials. The fact that no such resonance has been observed so far in the non-magnetic oxides points in the direction that the magnetism of Nd^{3+}, in particular the excitation of the 2.6 meV Kramers doublet, plays a role. A combination of site changes and different occupations of the Nd^{3+} spin states could also be responsible for the resonance besides the fluctuation of the occupation. Thus, dynamical processes related to the occupation of the first excited Kramers doublet of Nd^{3+} are the most likely interpretation of the resonance.

IV.   CONCLUSIONS

The μSR results for the present paramagnetic Nd_2O_3 sample are qualitative similar to data obtained for before-studied non-magnetic oxides.[29,32,36,37,39] The main component (in the present experiment 80 to 90% fraction) is a signal with a diamagnetic-like precession frequency but showing two different relaxations (moderate and slow). The moderately relaxing signal (sometimes called fast relaxing)[30,32,36] was heavy disputed in the past, assigned either to Mu^+ or Mu^- with delayed capture or loss of an electron. In a recent paper ((Ref. 30)) we gave a different interpretation of this state, i.e. assigned it to a weakly paramagnetic configuration which is formed as intermediate state between compact muonium and the final bound configuration where the muon is incorporated in the lattice structure. The present data are fully consistent with this transition state interpretation.

For the conversion of the moderate to slow fraction around 200 K a new formalism was developed which avoids ambiguities between fraction and relaxation in the transition region. In this analysis, the fraction and the re-

laxation are determined by a single parameter, the mean lifetime τ.

The present study on a paramagnetic sample reveals a resonance- like structure (the 40 K resonance), a feature not observed in previous experiments on non-magnetic oxides.[29,32,36,37,39] We assign this resonance behavior tentatively to the excitation of the first Kramers doublet of Nd^{3+} at 2.6 meV.[35,41,42] At 40 K, the ground and excited state are almost equally occupied but their population fluctuates. If this dynamical process comes into resonance with the muon Larmor precession, a spinlattice relaxation may give rise to a resonance behavior. A combination of electron site changes and different occupations of the Nd^{3+} spin states could also give rise to a fluctuating interaction. The present tentative assignment has to be checked by further experiments.

V.   ACKNOWLEDGEMENTS

* ruivilao@uc.pt

[1] G.-Y. Adachi, and N. Imanaka, The Binary Rare Earth Oxides, Chemical Reviews **98**, 1479 (1998).

[2] G. Adachi, N. Imanaka, and Z. C. Kang, Binary Rare Earth Oxides (Kluwer Academic Publishers, Dordrecht), Chap. 9. (2004)

[3] R. Gillen, and J. Robertson, Electronic structure of lanthanide oxide high K gate oxides, Microelectronic Engineering **109**, 72 (2013).

[4] G. Azimi, D. Dhiman, H.-M. Kwon, A. T. Paxson, and K. K. Varanasi, Hydrophobicity of rare-earth oxide ceramic, Nature Materials **12**, 315 (2013).

[5] E. Hemmer, N. Venkatachalam, H. Hyodo, A. Hattori, Y. Ebina, H. Kishimoto, and K. Soga, Upconverting and NIR emitting rare earth based nanostructures for NIR-bioimaging, Nanoscale **5**, 11339 (2013).

[6] K. H. Goh, A. S. M. A. Haseeb, and Y. H. Wong, Lanthanide rare earth oxide thin film as an alternative gate oxide, Materials Science in Semiconductor Processing **68**, 302 (2017).

[7] A. A. Dakhel, Characterisation of Nd_2O_3 thick gate dielectric for silicon, physica status solidi (a) **201**, 745 (2004).

[8] C. R. Michel, A. H. Martínez-Preciado, and N. L. López Contreras, Gas sensing properties of Nd_2O_3 nanostructured microspheres, Sensors and Actuators B: Chemical **184**, 8 (2013).

[9] R. Yuvakkumar, and S. I. Hong, Nd_2O_3: novel synthesis and characterization, Journal of Sol-Gel Science and Technology **73**, 511 (2015).

[10] A. Ramli, A. H. Shaari, H. Baqiah, H. B.C. S. Kean, M. M. A. Kechik, and Z. A. Talib, Role of Nd_2O_3 nanoparticles addition on microstructural and superconducting properties of $YBa_2Cu_3O_{7-\delta}$ ceramics, Journal of Rare Earths **34**, 895 (2016).

[11] S. H. Jeon, K. Nam, H. J. Yoon, Y.-I. Kim, D. W. Cho, and Y. Sohn, Hydrothermal synthesis of Nd_2O_3 nanorods, Ceramics International **43**, 1193 (2017).

[12] S. Zinatloo-Ajabshir, S. Mortazavi-Derazkola, and M. Salavati-Niasari, Nd_2O_3-SiO_2 nanocomposites: A simple sonochemical preparation, characterization and photocatalytic activity, Ultrasonics Sonochemistry **42**, 171 (2018).

[13] G. Sala, M. B. Stone, B. K. Rai, A. F. May, C. R. Dela Cruz, H. Suriya Arachchige, G. Ehlers, V. R. Fanelli, V. O. Garlea, M. D. Lumsden, D. Mandrus, and A. D. Christianson, Physical properties of the trigonal binary compound Nd_2O_3, Phys. Rev. Materials **2**, 114407 (2018).

[14] S. F. J. Cox, J. L. Gavartin, J. S. Lord, S. P. Cottrell, J. M. Gil, H. V. Alberto, J. Piroto Duarte, R. C. Vilão, N. Ayres de Campos, D. J. Keeble, E. A. Davis, M. Charlton, and D. P. van der Werf, Oxide muonics: II. Modelling the electrical activity of hydrogen in wide-gap and high-permittivity dielectrics, Journal of Physics: Condensed Matter **18**, 1079 (2006).

[15] S. F. J. Cox, Muonium as a model for interstitial hydrogen in the semiconducting and semimetallic elements, Reports on Progress in Physics **72**, 116501 (2009).

[16] S. F. J. Cox, R. L. Lichti, J. S. Lord, E. A. Davis, R. C. Vilão, J. M. Gil, T. D. Veal, and Y. G. Celebi, The first 25 years of semiconductor muonics at ISIS, modelling the electrical activity of hydrogen in inorganic semiconductors and high-κ dielectrics, Physica Scripta **88**, 068503 (2013).

[17] A. Weidinger, J. M. Gil, H. V. Alberto, R. C. Vilão, J. Piroto Duarte, N. Ayres de Campos, and S. F. J. Cox, Shallow donor versus deep acceptor state in II−VI semiconductor compounds, Physica B: Condensed Matter **326**, 124 (2003).

[18] R. L. Lichti, K. H. Chow, J. M. Gil, D. L. Stripe, R. C. Vilão, and S. F. J. Cox, Location of the H $[+/-]$ level: Experimental limits for muonium, Physica B **376-377**, 587 (2006).

[19] T. Liu, Y. Zhang, H. Li, and X. Shao, Synthesis and Characteristics of Sm_2O_3 and Nd_2O_3 Nanoparticles, Langmuir **19**, 7569 (2003).

[20] J. Päiväsaari, M. Putkonen, and L. Niinistö, A comparative study on lanthanide oxide thin films grown by atomic layer deposition, Thin Solid Film **472**, 275 (2005).

[21] R. C. Vilão, J. M. Gil, A. Weidinger, H. V. Alberto, J. Piroto Duarte, N. Ayres de Campos, R. L. Lichti, K. H. Chow, and S. F. J. Cox, Information on hydrogen states in IIVI semiconductor compounds from a study of their muonium analogues, Nuclear Instruments and Methods in Physics Research Section A: Accelerators, Spectrometers, Detectors and Associated Equipment **580**, 438 (2007).

[22] R. C. Vilão, R. B. L. Vieira, H. V. Alberto, J. M. Gil, A. Weidinger, R. L. Lichti, B. B. Baker, P. W. Mengyan, and J. S. Lord, Muonium donor in rutile TiO_2 and comparison with hydrogen, Physical Review B **92**, 081202(R) (2015).

[23] A. G. Marinopoulos, Incorporation and migration of hydrogen in yttria-stabilized cubic zirconia: Insights from semilocal and hybrid-functional calculations, Physical Review B **86**, 155144 (2012).

[24] A. G. Marinopoulos, Protons in cubic yttria-stabilized zirconia: Binding sites and migration pathways, Solid State Ionics **315**, 116 (2017).

[25] A. G. Marinopoulos, R. C. Vilão, H. V. Vieira, H. V. Alberto, J. M. Gil, M. V. Yakushev, R. Scheuermann, and T. Goko, Defect levels and hyperfine constants of hydrogen in beryllium oxide from hybrid-functional calculations and muonium spectroscopy, Philosophical Magazine **97**, 2108 (2017).

[26] A. G. Marinopoulos, R. C. Vilão, H. V. Alberto, and J. M. Gil, Electronic structure and migration of interstitial hydrogen in the rutile phase of TiO_2, Journal of Physics: Condensed Matter **30**, 425503 (2018).

[27] S. F. J. Cox, E. A. Davis, S. P. Cottrell, P. J. C. King, J. S. Lord, J. M. Gil, H. V. Alberto, R. C. Vilão, J. Piroto Duarte, N. Ayres de Campos, A. Weidinger, R. L. Lichti, and S. J. C. Irvine, Experimental Confirmation of the Predicted Shallow Donor Hydrogen State in Zinc Oxide, Phys. Rev. Lett. **86**, 2601 (2001).

[28] P. D. C. King, R. L. Lichti, Y. G. Celebi, J. M. Gil, R. C. Vilão, H. V. Alberto, J. Piroto Duarte, D. J. Payne, R. G. Egdell, I. McKenzie, C. F. McConville, S. F. J. Cox, and T. D. Veal, Shallow donor state of hydrogen in In_2O_3 and SnO_2: Implications for conductivity in transparent conducting oxides, Phys. Rev. B **80**, 081201(R) (2009).

[29] E. L. da Silva, A. G. Marinopoulos, R. B. L. Vieira, R. C. Vilão, H. V. Alberto, J. M. Gil, R. L. Lichti, P. W. Mengyan, and B. B. Baker, Electronic structure of interstitial hydrogen in lutetium oxide from $DFT + U$ calculations and comparison study with μSR spectroscopy, Phys. Rev. B **94**, 014104 (2016).

[30] R. C. Vilão, R. B. L. Vieira, H. V. Alberto, J. M. Gil, and A. Weidinger, Role of the transition state in muon implantation, Phys. Rev. B **96**, 195205 (2017).

[31] R. C. Vilão, R. B. L. Vieira, H. V. Alberto, J. M. Gil, A. Weidinger, R. L. Lichti, P. W. Mengyan, B. Baker, and J. S. Lord, Barrier model in muon implantation and application to Lu_2O_3, Phys. Rev. B **98**, 115201 (2018).

[32] R. C. Vilão, H. V. Alberto, J. M. Gil, and A. Weidinger, Thermal spike in muon implantation, Physical Review B **99**, 195206 (2019).

[33] P. Villars and L. D. Calvert, Pearsons Handbook of Crystallographic Data for Intermetallic Phases, 2nd ed. (ASM International,Ohio) (1991).

[34] T. Bernier, Y. Lejus, H. Tueta, and X. Collongues, Susceptibilite paramagnetique anisotrope de monocristaux d'oxyds Nd_2O_3 et $La_xNd_{2-x}O_3$, Materials Research Bulletin **8**, 261 (1973).

[35] P. Caro, J. Derouet, L. Beaury, and E. Soulie, Interpretation of the optical absorption spectrum and of the paramagnetic susceptibility of neodymium Atype sesquioxide, The Journal of Chemical Physics **70**, 2542 (1979).

[36] R. C. Vilão, A. G. Marinopoulos, R. B. L. Vieira, A. Weidinger, H. V. Alberto, J. P. Duarte, J. M. Gil, J. S. Lord, and S. F. J. Cox, Hydrogen impurity in paratellurite $\alpha-TeO_2$: Muon-spin rotation and ab initio studies, Phys. Rev. B **84**, 045201 (2011).

[37] R. B. L. Vieira, R. C. Vilão, A. G. Marinopoulos, P. M. Gordo, J. A. Paixão, H. V. Alberto, J. M. Gil, A. Weidinger, R. L. Lichti, B. Baker, P. W. Mengyan, and J. S. Lord, Isolated hydrogen configurations in zirconia as seen by muon spin spectroscopy and *ab initio* calculations, Phys. Rev. B **94**, 115207 (2016).

[38] H. V. Alberto, R. C. Vilão, R. B. L. Vieira, J. M. Gil, A. Weidinger, M. G. Sousa, J. P. Teixeira, A. F. da Cunha, P. M. P. Salomé, P. A. Fernandes, T. Törndahl, T. Prokscha, A. Suter, and Z. Salman, Slow-muon study of quaternary solar-cell materials: Single layers and $p-n$ junctions, Phys. Rev. Materials **2**, 025402 (2018).

[39] E. L. Silva, A. G. Marinopoulos, R. C. Vilão, R. B. L. Vieira, H. V. Alberto, J. Piroto Duarte, and J. M. Gil, Hydrogen impurity in yttria: *Ab initio* and μSR perspectives, Physical Review B **85**, 165211 (2012).

[40] R. B. L. Vieira, R. C. Vilão, P. M. Gordo, A. G. Marinopoulos, H. V. Alberto, J. Piroto Duarte, J. M. Gil, A. Weidinger, and J. S. Lord, Muon-Spin-Rotation study of yttria-stabilized zirconia (ZrO_2:Y): Evidence for muon and electron separate traps, Journal of Physics: Conference Series **551**, 012050 (2014).

[41] J. R. Henderson, M. Muramoto, and J. B. Gruber, Spectrum of Nd^{3+} in Lanthanide Oxide Crystals, The Journal of Chemical Physics **46**, 2515 (1967).

[42] B. H. Justice, and E. F. Westrum, Thermophysical properties of the lanthanide oxides. I. Heat capacities, thermodynamic properties, and some energy levels of lanthanum (iii) and neodymium (iii) oxides from 5 to 350 K , J. Phys. Chem. **67**, 339 (1963).